EuroGNC Navigation Guidance Control CEAS Bristol, UK June 11th-13th 2024
University of BRISTOL ROYAL AERONAUTICAL SOCIETY AIAA

Navigation Algorithm for a Twin-Engine Turboprop Aircraft using an Extended Kalman Filter

Mushfiqul Alam Lecturer in Flight Dynamics, Centre for Aeronautics, School of Aerospace, Transport and Manufacturing, Cranfield University, Bedford, MK430AL, United Kingdom. mushfiqul.alam@cranfield.ac.uk

James Whidborne Professor in Control Engineering, Centre for Aeronautics, School of Aerospace, Transport and Manufacturing, Cranfield University, Bedford, MK430AL, United Kingdom. j.f.whidborne@cranfield.ac.uk

Mark Westwood Professor in Aeronautics, Centre for Aeronautics, School of Aerospace, Transport and Manufacturing, Cranfield University, Bedford, MK430AL, United Kingdom. mark.westwood@cranfield.ac.uk

ABSTRACT

MEMS ((micro-electro-mechanical system) based sensing technologies have garnered interest in replacing the traditionally heavy and expensive ring laser gyros and servo accelerometers used in inertial measurement unit (IMU) for obtaining position/velocity and attitude estimates. A strapdown MEMS bases IMU consists of tri-axial accelerometers (ACCs) and tri-axial angular rate sensors (ARSs) often aided with GNSS measurements. MEMS based sensors suffer from stochastic errors such as bias instability which needs to be considered during the estimation of the navigation data. This paper presents a dual stage cascaded extended Kalman filtering (EKF) framework for fusing the ACC and ARS measurement with the GNSS measurements. Additionally, vehicle true airspeed data is used for the estimation of air data such as angle of attack and sideslip. The performance of the EKF based navigation algorithm is tested using the Saab 340B twin engine turboprop aircraft operated by the Cranfield University's National Flying Laboratory Centre (NFLC). In-flight dynamic maneuvers were performed following the DO-334 - Minimum Operational Performance Standards (MOPS) for Strapdown Attitude and Heading Reference Systems (AHRS) for collecting data to assess the performance of the navigation algorithm. From the maneuvers performed, the assessment shows the performance of the attitude estimation meets the requirements in terms of ensuring accuracy.

Keywords: nonlinear navigation; extended Kalman filter; INS/GNSS sensor fusion, MEMS sensors, DO-334 standard; air data estimation

Nomenclature

$a_{x_m}, a_{y_m}, a_{z_m}$	=	Body acceleration in x, y, and z axis measured by the sensor (g)
$ae_{bx}, ae_{by}, ae_{bz}$	=	External linear body acceleration in in x, y, and z axis. (m/s^2)
$b_{g_x}, b_{g_y}, b_{g_z}$	=	Angular rate sensor bias in x, y, and z-axis (rad/s)
$b_{a_x}, b_{a_y}, b_{a_z}$	=	Accelerometer sensor bias in x, y, and z-axis (g)
u, v, w	=	Velocity in the body-frame (m/s)
P_N, P_E, P_D	=	Position in North, East and Down (m)
V_N, V_E, V_D	=	Velocity in North, East and Down (m/s)

V_o	=	True air speed (m/s)
$\omega_{x_m}, \omega_{y_m}, \omega_{z_m}$	=	Body angular rate in x, y, and z axis measured by the sensor (rad/s)
Φ, θ, ψ	=	Euler angles (roll, pitch, heading) (rad)
$\boldsymbol{x}, \boldsymbol{u}, \boldsymbol{z}$	=	States, input and measurement of the extended Kalman filter
^	=	Denotes the prediction step of the Kalman filter

1 Introduction

Through the development of MEMS ((micro-electro-mechanical system) based sensing technologies there is a renewed interest in replacing the traditionally heavy and expensive ring laser gyros and servo accelerometers used in inertial measurement unit (IMU) with MEMS based IMUs. A strapdown inertial system consisting of tri-axial accelerometers (ACCs) and tri-axial angular rate sensors (ARSs) is commonly used for attitude (roll, pitch, yaw angle), as well as for position and velocity evaluations (the so-called PVA estimates) [1]. MEMS-based inertial sensors suffer from deterministic errors and stochastic errors. Deterministic errors such as scale factor, misalignment and nonorthogonality can be corrected using simple laboratory experiments such as those using a "Rotational Tilt Platform" [2]. Stochastic errors such as bias instability need to be considered in the real time data processing which presents a considerable challenge in the navigation data estimation processes [3], [4], [5].

The attitude and heading reference system (AHRS) is formed using estimated attitude by integrating angular rates (ARS measurements), primarily aided by the ACC measurements. Heading estimation in the AHRS is traditionally aided by magnetometers. However, magnetometers are sensitive to hard and soft iron effects [1]. With the availability of the Global Navigation Satellite System (GNSS) measurements the heading angle can be obtained using the GNSS measurements. The position and velocity (PV) estimates can be obtained by integrating the ACC measurements, the so-called dead-reckoning process. Due to the stochastic errors in MEMS-based sensors, dead reckoning cause unbounded error growth, which needs to be corrected using the position aids obtained from Global Navigation Satellite System (GNSS) measurements [6]. The aiding of IMUs measurements using GNSS to obtain PVA estimates is called INS/GNSS navigation solutions.

There have been several navigation algorithm proposed for fusing INS/GNSS in order to obtain PVA estimates, such as temporally interconnected observers [7], complementary filters or Kalman filters (KF) and extended Kalman Filter (EKF) with various architectures [4], [8], [9], nonlinear observers (NLO) [10], unscented Kalman filters (UKF) and particle filters (PF) [11] and eXogenous Kalman Filter [12].

The authors previously suggested a navigation algorithm framework for PVA estimates using a dual structured EKF for PVA estimation where the attitude estimation filter is cascaded with a PV estimation filter [6]. This cascaded navigation algorithm avoids the need to propagate additional states, resulting in the covariance propagation becoming computationally efficient [6]. The proposed navigations extend the framework to include the air data estimates such as angle of attack (AoA) (α) and angle of sideslip (AoS) (β). Even if the aircraft is equipped with an AoA and AoS sensor, it is essential to have an estimator for α and β, since the AoA and AoS sensors are known to be prone to error and can provide erroneous readings. For example, feeding erroneous AoA measurements contributed to several air accidents [13], [14]. A details survey on the measurements and estimation of AoA and AoS can be found in Ref [15], [16], [17].

The purpose of this article is to develop a navigation algorithm using nonlinear estimation technique, specifically extended Kalman Filter whose performance is assessed against the dynamic maneuvers for

longitudinal and lateral-directional motion such as pitch up/down, short-period, long-period, steady-sideslip, sharp turn, etc. which are required in DO-334 standards [18].

The proposed navigation algorithm is tested using the Cranfield University Saab 340B twin-engine turbo aircraft (see Fig. 1a), called Flying Laboratory operated by the National Flying Laboratory Centre (NFLC). The flying platform offers a unique facility to validate the performance of such estimation framework. The aircraft has gone through a series of modifications to include various teaching, research and experimental equipment including a MEMS based IMU sensors called Ekinox-D: Dual GPS INS [19], GNSS receiver and a set of AoA and AoS sensors (see Fig. 1b).

(a) Cranfield's Saab 340B National Flying Laboratory **(b) Installed AoA and AoS sensors.**

Fig. 1. Saab 340B operated by the NFLC.

The performance of the navigation algorithm using the MEMS-based IMU and GNSS measurements is compared against the Saab 340B onboard analogue Flight Data Acquisition System which uses Rockwell Collins AHRS 3000 IMU unit [20]. Additionally, the performance of the air data estimates is compared with the α and β measurements.

The rest of the paper is organized as follows: Section 2 outlines the principles of proposed dual stage navigation algorithm using the extended Kalman filter. Section 3 presents the data acquisition system, flight test platform and experimental setup. Section 4 presents details analysis of the results and discussion. Finally concluding the paper with final remarks.

2 Principles of the Navigation Algorithm

A loosely coupled navigation algorithm using multi-stage EKF architecture is proposed. The overall estimation process is divided into two main sections: an Attitude estimator and a Position/Velocity with air data estimator. By using cascaded Kalman filtering, this method avoids the need to propagate additional states making the algorithm computationally efficient. Keeping the number of states in the estimator to a minimum, the tuning of the EKF becomes less complex. Additionally, the modular structure of the proposed framework makes the addition of extra aiding sources to the Attitude estimator and/or the PV estimator straight forward keeping the core framework the same.

The novelty in the proposed algorithms lies in the inclusion of air data estimates in addition to the PVA estimates. The overall estimation process is shown in a block scheme in Fig. 2. In the following sections, each part of the estimator structure is introduced in detail.

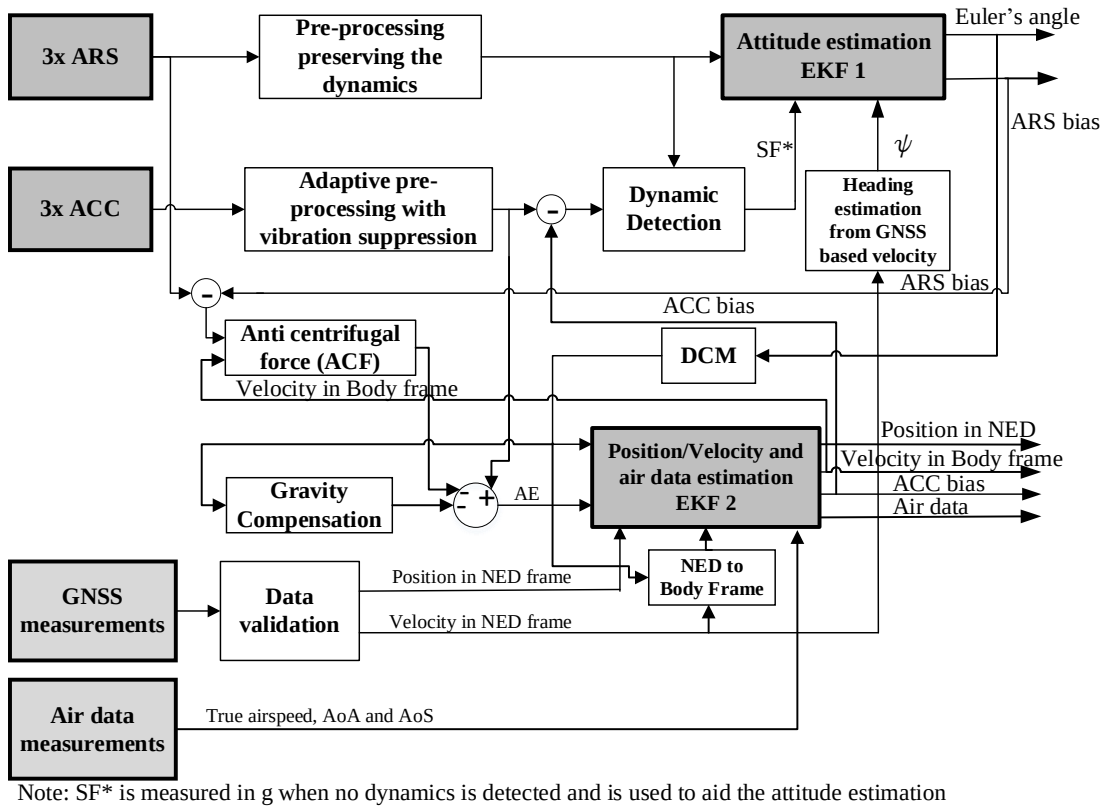

Note: SF* is measured in g when no dynamics is detected and is used to aid the attitude estimation
AE is the external linear acceleration

Fig. 2. IMU/GNSS loosely coupled integration scheme using a dual structure EKF estimator.

The traditional axis system is used for developing the navigation algorithm where the x-axis points towards the nose of the aircraft, the y-axis points towards the starboard and z-axis points downwards.

2.1 EKF Based Attitude Estimator

The aircraft/vehicle attitude is represented in this case by Euler angles since we assume singularity free calculations. This assumption comes from the operation conditions and limits of most commercial aircraft. The state vector $\boldsymbol{x}$ and input $\boldsymbol{u}$ are defined by

$$\boldsymbol{x} = \left[\phi, \theta, \psi, b_{g_x}, b_{g_y}, b_{g_z}\right]^T, \boldsymbol{u} = \left[\, \omega_{x_m}, \omega_{y_m}, \omega_{z_m}\right]^T \tag{1}$$

and $\boldsymbol{x}$ is updated using the input $\boldsymbol{u}$ along with the following the EKF model

$$\dot{\boldsymbol{x}} = \boldsymbol{f}\left(\begin{bmatrix} 1 & \sin\phi\tan\theta & \cos\phi\tan\theta \\ 0 & \cos\phi & -\sin\phi \\ 0 & \sin\phi\sec\theta & \cos\phi\sec\theta \end{bmatrix}\left(\begin{bmatrix} \omega_{x_m} \\ \omega_{y_m} \\ \omega_{z_m} \end{bmatrix} - \begin{bmatrix} b_{g_x} \\ b_{g_y} \\ b_{g_z} \end{bmatrix}\right)\right) \tag{2}$$
$$\begin{matrix} 0 \\ 0 \\ 0 \end{matrix}$$

It is assumed that the bias of the ARS sensors varies very slowly and the rate of change of ARS biases are approximated as zero.

The expected measurements prediction vector, $\hat{\boldsymbol{z}}$ given by

$$\hat{\boldsymbol{z}} = \begin{bmatrix} \sin\theta \\ -\cos\theta\,\sin\phi \\ -\cos\phi\,\sin\theta \\ \psi \end{bmatrix} \tag{3}$$

is related to the ACC readings when the ACC measurement is not affected by external acceleration and is subject to only gravity, which means steady state, equilibrium motion. The measurement, $\boldsymbol{z}$ is given by:

$$\boldsymbol{z} = \begin{bmatrix} a_{x_m} \\ a_{y_m} \\ a_{z_m} \\ \psi_{GNSS} \end{bmatrix} \tag{4}$$

The heading (ψ) is evaluated based on the GNSS velocities as:

$$\psi_{GNSS} = \text{atan2}\left(V_{GNSS_{East}}, V_{GNSS_{North}}\right) \tag{5}$$

and is used for aiding when following condition is fulfilled

$$norm_{Vel_{GNSS}} = \sqrt{V_{GNSS_{North}}^2 + V_{GNSS_{East}}^2 + V_{GNSS_{Down}}^2} > 5\ m/s \tag{6}$$

We note that usage of GNSS velocities provides the course (track) angle, which is equal to the heading angle only when the sideslip angle is zero. This assumption leads to a reasonable approximation when winds and turns are not too large. If the $norm_{Vel_{GNSS}}$ is less than 5 m/s (approx. 10kts), then the heading estimation based on GNSS velocity is noisy. If the ACC and ARS readings are affected by vibration arising from the vehicle structures, an adaptive pre-processing can be applied before the data are used inside EKF, for details on adaptive filtering for reducing vibration impact please see Ref [3].

As shown in the block diagram in Fig. 2, the ARS bias is fed back to the ARS input. The detection of dynamics is important because if the ACC measurements are used to correct the attitude estimated when the aircraft was not in a steady-state condition then the attitudes will be wrongly corrected. The ACC data are only used as measurement to correct the attitude whenever there is no significant dynamics detected in the vehicle motion.

2.2 Dynamic Detection

For the ACC based aiding in an attitude estimator it is important to recognize conditions under which ACC readings are affected by only gravity, which means no dynamic change in the motion. For this purpose, we have designed a dynamics detector formed by three parameters which are monitored simultaneously from data history. In our case it was set to a history window of 2 seconds. These monitoring parameters are:

1. The norm of the ACC readings

$$ACC_{norm} = \sqrt{a_{x_m}^2 + a_{y_m}^2 + a_{z_m}^2} \tag{7}$$

2. The norm of the ARS data

$$ARS_{norm} = \sqrt{\left(\omega_{\mathrm{x_m}} - b_{g_x}\right)^2 + \left(\omega_{\mathrm{y_m}} - b_{g_y}\right)^2 + \left(\omega_{\mathrm{z_m}} - b_{g_z}\right)^2} \tag{8}$$

3. The rate of heading change

$$\dot{\psi} = \left(\frac{\left(\omega_{y_m} - b_{g_y}\right)\sin\phi}{\cos\theta} + \frac{\left(\omega_{z_m} - b_{g_z}\right)\cos\phi}{\cos\theta} \right) \tag{9}$$

In an ideal case only ACC_{norm} can be monitored for detecting dynamics; and when it equals to 1g, no dynamic conditions could be considered. However, under real operating conditions under harsh environment bounds/thresholds should be set to allow possibility for variation along with monitoring the parameters from (7)-(9). We have thus considered the following conditions and no dynamic motion is assumed to be present when all three conditions are met simultaneously.

Condition 1: $|ACC_{norm} - 1g| < threshold_{ACC}$.

Condition 2: $|GYR_{norm}| < threshold_{GYR}$.

Condition 3: $|\dot{\psi}| < threshold_{ARS}$.

The threshold values are chosen depending on a vehicle type and/or adaptively modified according to operational conditions. The three parameters from (7)-(9) are monitored for 2 seconds from the history of the estimation, when all conditions 1-3 are met throughout 2 second window, it is considered that ACC output is affected just by gravity and thus ACC based attitude estimation is used for compensating the attitude obtained primarily by free integration of ARS data.

2.3 EKF Based Position/Velocity and Air Data Estimator

The estimator estimates position in the NED frame (P_N, P_E, D_D), velocity in the body-frame (u, v, w) and ACC bias (b_{ax}, b_{ay}, b_{az}) in the body frame while using GNSS position and velocity as aiding measurements in addition to the true airspeed (V_o) and α and β measured by the aircraft's pitot-static tube and AoA and AoS probes. The state vector, $\boldsymbol{x}$ i and input $\boldsymbol{u}$ iare

$$\boldsymbol{x} = \left[P_N, P_E, P_D, u, v, w, b_{a_x}, b_{a_y}, b_{a_z}, \alpha, \beta\right]^T, \boldsymbol{u} = \left[\, ae_{bx}, ae_{by}, ae_{bz},\ \boldsymbol{C_b^n}\right]^T \tag{10}$$

and $\boldsymbol{x}$ is updated using $\boldsymbol{u}$ and the following the EKF model

$$\dot{\boldsymbol{x}} = \boldsymbol{f}\begin{pmatrix} \boldsymbol{C_b^n}\begin{bmatrix} u \\ v \\ w \end{bmatrix} \\ \begin{bmatrix} ae_{bx} \\ ae_{by} \\ ae_{bz} \end{bmatrix} - \begin{bmatrix} b_{a_x} \\ b_{a_y} \\ b_{a_z} \end{bmatrix} \\ 0 \\ 0 \\ 0 \\ \dfrac{u\left(ae_{bz} - b_{a_z}\right) - w(ae_{bx} - b_{a_x})}{u^2 + w^2} \\ \dfrac{u\left(ae_{by} - b_{a_y}\right) - v(ae_{bx} - b_{a_x})}{u^2 + v^2} \end{pmatrix} \tag{11}$$

Here $\boldsymbol{C_b^n}$ is the direction cosine matrix transforming the body-frame to NED navigation frame. The inputs $ae_{bx}, ae_{by}, ae_{bz}$ in eq (10) are calculated as:

$$\begin{bmatrix} ae_{bx} \\ ae_{by} \\ ae_{bz} \end{bmatrix} = \begin{bmatrix} a_{x_m} \\ a_{y_m} \\ a_{z_m} \end{bmatrix} g - \boldsymbol{C_b^n}\begin{bmatrix} 0 \\ 0 \\ 1 \end{bmatrix} + \boldsymbol{ACF} \tag{12}$$

The $\boldsymbol{ACF}$ is the anti-centrifugal force experienced by the vehicle and is calculated as:

$$\boldsymbol{ACF} = \begin{pmatrix} v\left(\omega_{z_m} - b_{g_z}\right) - w\left(\omega_{y_m} - b_{g_y}\right) \\ -u\left(\omega_{z_m} - b_{g_z}\right) + w\left(\omega_{x_m} - b_{g_x}\right) \\ u\left(\omega_{y_m} - b_{g_y}\right) - v\left(\omega_{x_m} - b_{g_m}\right) \end{pmatrix} \tag{13}$$

The expected measurements prediction, $\hat{\boldsymbol{z}}$ and measurement, $\boldsymbol{z}$ are given by:

$$\hat{\boldsymbol{z}} = \begin{bmatrix} P_N \\ P_E \\ P_D \\ \boldsymbol{C_b^n}\begin{bmatrix} u \\ v \\ w \end{bmatrix} \\ \sqrt{u^2 + v^2 + w^2} \\ \alpha \\ \beta \end{bmatrix}; \ \mathbf{z} = \begin{bmatrix} P_N \\ P_E \\ P_D \\ V_N \\ V_E \\ V_D \\ V_o \\ \alpha \\ \beta \end{bmatrix} \tag{14}$$

As shown in the estimation block diagram in Fig. 2, it is important to validate GNSS data before they are processed. Any bad sample from the GNSS data may cause an inaccurate estimation of the state vector. The details of the method on GNSS data validation can be found in Ref [6].

3 Data Acquisition, Experimental Setup and Flight Testing

This section provides an overview of the data acquisition unit, flight test platform and experimental setup.

3.1 Experimental Platform

The flight experiment is conducted using the Cranfield University's National Flying Laboratory - G-NFLB Saab 340B aircraft, shown in Fig. 1. The Saab 340B is a turboprop with a maximum take-off weight of 13155 kg, powered by two GE CT7-9B engines (maximum continuous rating 1750 SHP). It has been converted into a laboratory for in-flight experimental work by the installation of an instrumentation system and seat-back displays. The cabin layout in G-NFLB is configured to 33 seats, although the normal maximum seating capacity of 24 is used. The on-board instrumentation system consists of signal conditioning units, power supplies, an Inertial Management Unit (IMU) and a data acquisition system.

3.2 Data Acquisition Unit

The original aircraft was modified to add instrumentation for use as a flying laboratory. The forward galley was removed and replaced with an equipment rack containing computer, data acquisition unit and other onboard instrumentation shown in Fig. 3.

Within the sets of additional instruments there is a MEMS based inertial measurements unit called Ekinox-D. Ekinox-D is a tactical grade compact high end MEMS sensor. The advanced INS/GNSS comes with one or two antennas and provides orientation, heave, and centimeter-level position when aided with real time kinematics (RTK) based GNSS positioning. Ekinox sensors are embedded with an 8 GB data logger for post-operation analysis or post-processing.

The aircraft is additionally retro fitted with 861CAR Rosemount AoA and AoS vanes shown in Fig. 1b. Two AoS probes are fitted, one on the left and one on the right side. The Curtis Wright's KAM-500 is used for the analogue data acquisition of on-board Saab 340B instruments such as Rockwell Collins AHRS 3000 IMU unit as well as other aircraft parameters such as control surface deflections and control stick positions using the Commercial Standard Digital Bus (CSDB) protocol. The attitude and heading reference information obtained from the CSDB protocol is used as a reference for comparing the performance the proposed navigation algorithm.

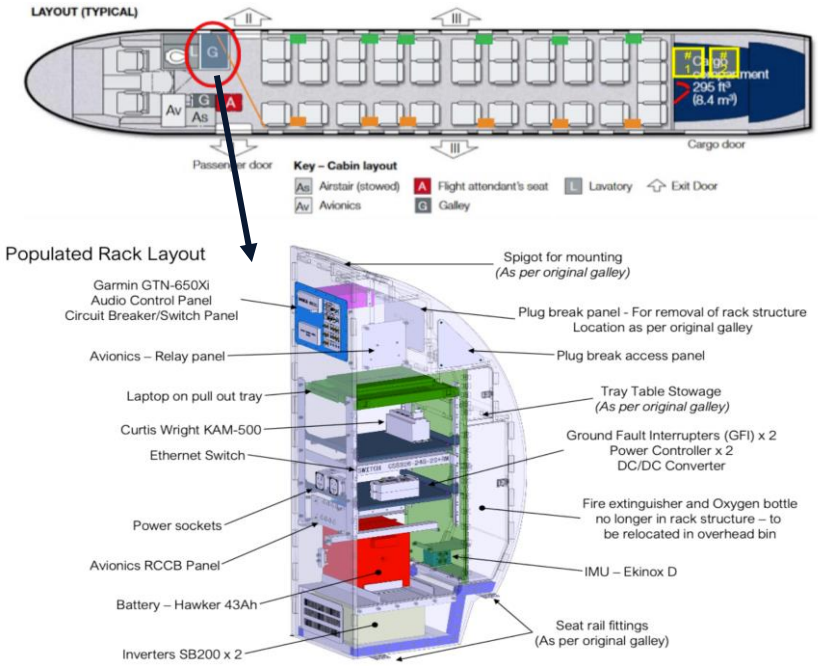

Fig. 3. Overview of NFLC's Saab 340B instrumentation.

3.3 Experimental Setup and Flight Testing

The experimental flight included various flight patterns including slow turns and rapid altitude changes. The flight includes rolling, take-off, climb cruise, descent, landing, and other additional dynamic maneuvers such as Phugoid and roll mode as mentioned in the DO-334 standard as shown in Fig. 4.

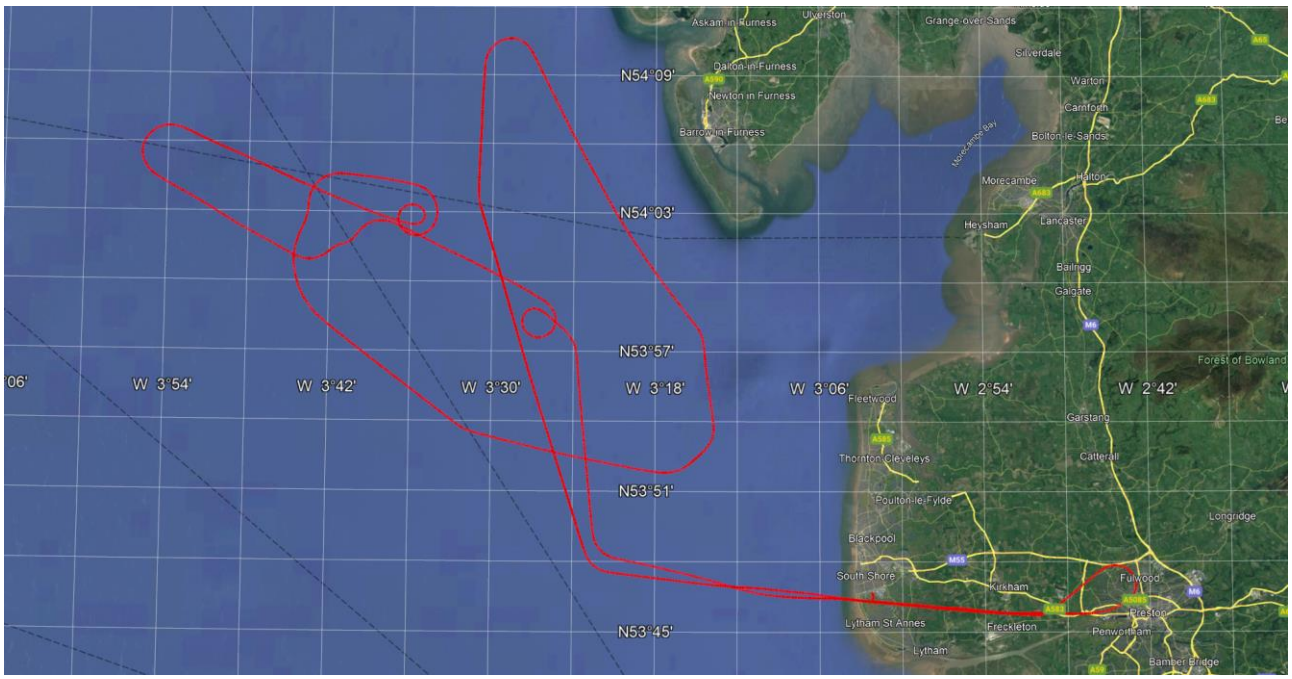

(a) 2D trajectory projection on the Google Map of the flight test performed.

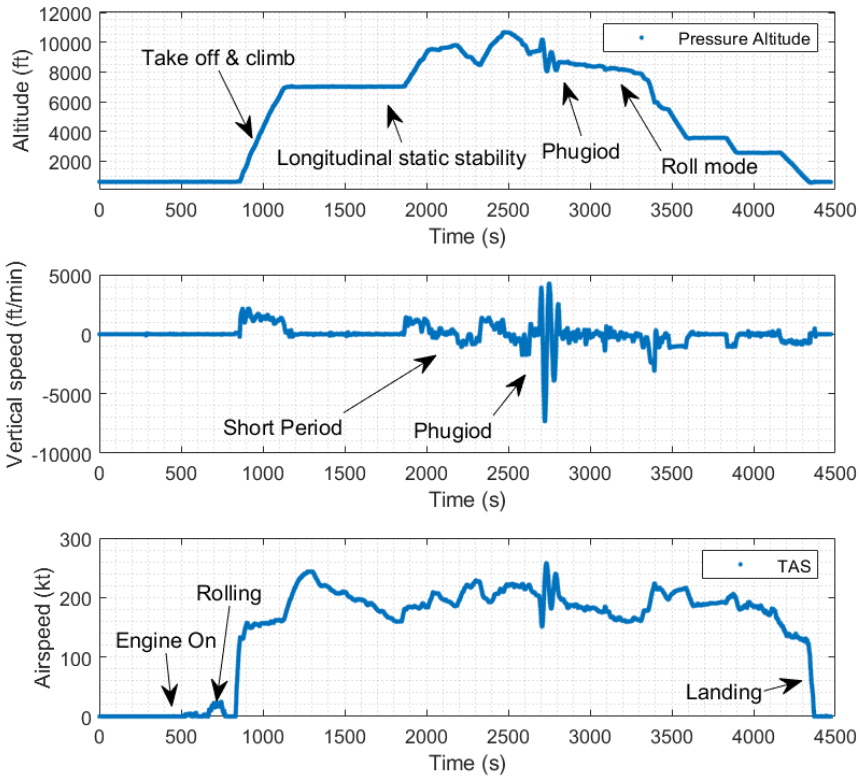

(b) Altitude profile of the flight along with other air parameters.

Fig. 4. Flight test trajectory.

4 Results and Discussion

4.1 Attitude Estimation

This section presents the estimation results of the proposed cascaded dual stage navigation algorithm using EKF. The attitude information obtained from the CSDB data acquisition system is used as a reference for comparison with the EKF estimates. Additionally, the commercially available Ekinox-D IMU unit estimation is compared. The attitude estimates are shown in Fig. 5. In Fig. 5b it can be seen that the ARS biases vary slowly. The innovation plot for the estimator is presented in Appendix A.

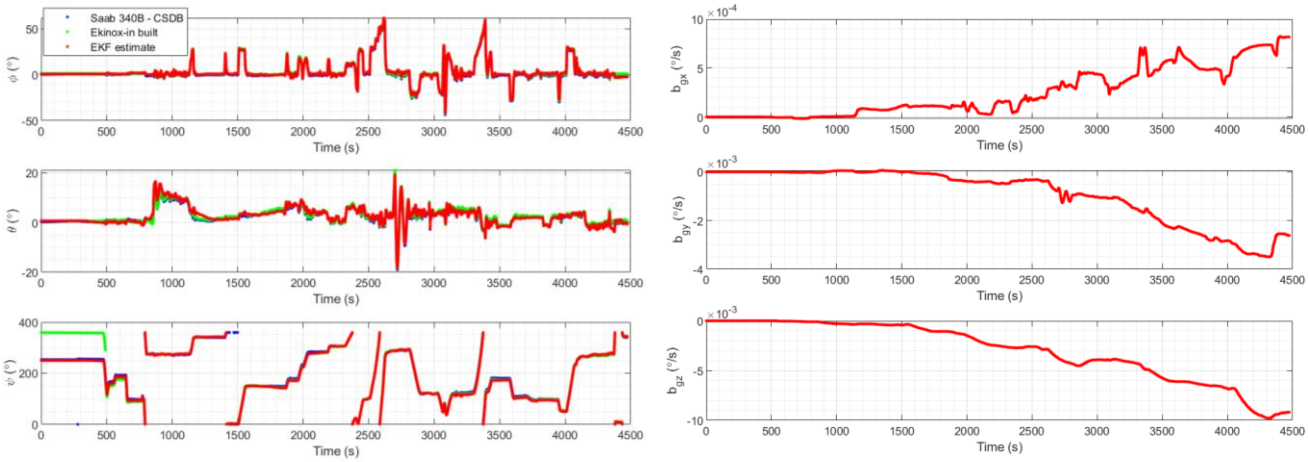

(a) Attiude estimate **(b) Estimated ARS bias**

Fig. 5. Attitude estimation from the Attitude Estimator.

The evaluation of the attitude estimates is evaluated using the DO-334 standards. The requirements state that under dynamic conditions for the Category 4 AHRS aided heading system with GNSS the root mean

squared error (RMSE) of attitude (ϕ and θ) when compared to the reference system must be less than twice the 2.5^o and less than twice 6^o for heading (ψ) [18]. The RMSE of the attitude and heading estimate is presented in Table 1. The RMSE of the EKF estimates is calculated with respect to the Saab 340B's internal instrumentation obtained via CSDB.

Table 1. Evaluation of attitude and heading performance for the EKF estimator compared to aircraft onboard instrument measurements.

Flight Evaluation Profile: Standard Maneuvers					
			RMSE (°)		
No.	**Maneuvers**	**Condition**	$\boldsymbol{\phi}$	$\boldsymbol{\theta}$	$\boldsymbol{\psi}$
1	Taxi, take-off, climb	Standard take off speed	0.78	1.43	5.42
2	Straight and level	5 mins	0.38	0.58	2.74
3	Standard rate right turn	360° heading change	1.43	1.05	5.25
4	Phugoid mode		2.73	1.44	2.3
5	Roll mode (steep bank angle)	Up to 50°	1.18	0.84	5.04
6	Approach and landing	Standard landing speed	1.40	1.07	5.56

From Table 1 it can be seen that the EKF based attitude and heading estimator produces RMSE which are below specified limits for the presented dynamic maneuvers, meeting the Category 4 criteria.

4.2 Position/Velocity and Air Data Estimation

There were no reference data available for comparing the position estimates. The position and velocity estimates are compared with the single point GPS measurements. Fig. 6 presents the position and velocity estimates.

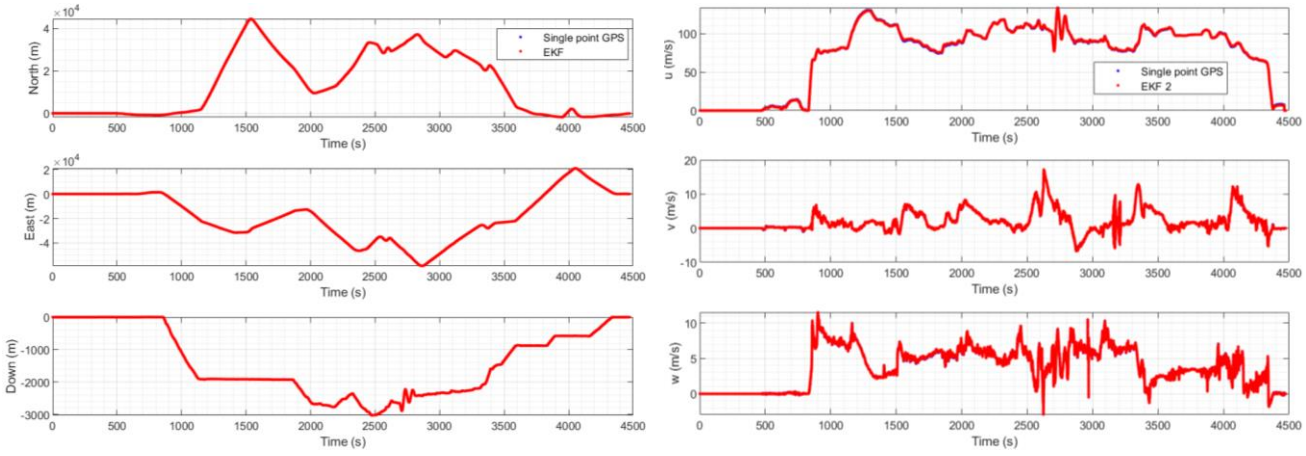

(a) Position estimates. **(b) Velocity estimates.**

Fig. 6. Position and Velocity estimates using the Position/Velocity air data estimator.

For the comparison purposes the α and β was calculated using Eq (15)-(16).

$$\alpha = \tan^{-1}\left(\frac{w}{u}\right) \tag{15}$$

$$\beta = \tan^{-1}\left(\frac{v}{u}\right) \tag{16}$$

The estimated air data, the measured air data and calculated air data from the estimates is plotted in Fig. 7a. The ACC bias estimates are shown in Fig. 7b.

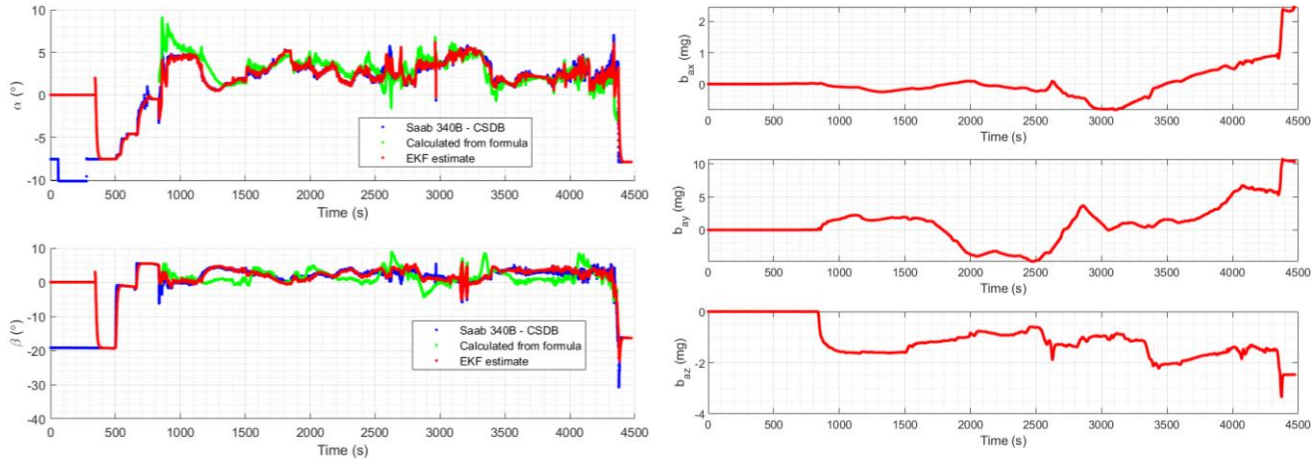

(a) Air data estimates. **(b) ACC bias estimates.**

Fig. 7. Air data and ACC bias estimates using the Position/Velocity and Air data estimator.

In Fig. 7a, at the beginning of the flight, the measured α and β values start from non-zero position. It is because the installed AoA and AoS sensor were floating vent type, hence they only provide reliable measurement when the airspeed is large enough. The calculated α and β using Eq (15) and (16) overestimates the air data. In contrast it can be seen the EKF estimates slowly converges to the measured α and β. It is worth noting here, that the convergence of the estimated α and β is slow because the tuning value chosen for the measurement covariance is relatively large, (see Appendix C for tuning values). This is chosen intentionally to avoid erroneous estimates in the case of faulty measurements. The innovation plots of the estimator are presented in Appendix B.

Conclusions

The paper presented a modular framework for INS/GNSS and air data fusion using dual stage cascaded extended Kalman filter (EKF) for obtaining attitude, position/velocity and air data estimates. The navigation algorithm is tested using the Saab 340B twin-engine turboprop aircraft operated by the Cranfield University's National Flying Laboratory Centre (NFLC). A specific flight test was conducted to include the dynamic maneuvers listed in DO-344 standards for the performance evaluation of the navigation algorithm. The performance evaluation shows that the attitude and heading estimates meet the requirements mentioned in the standard. However, the position and velocity estimates could not be quantified due to the lack of reference data. Future work will include expanding the scope of the flight test and obtain reference position and velocity estimates for the assessment of position estimates.

Acknowledgments

The authors would like to thank Dr. Simon Place, Robert Harrison, and Joe Brown at the Cranfield University's National Flying Laboratory Centre for flying the aircraft, obtaining and provision of the flight data. This research is part funded through the project Out of Cycle NExt generation highly efficient air transport (ONEheart) by Innovate UK.

References

[1] D. Titterton and J. L. Weston, *Strapdown inertial navigation technology*, vol. 17. IET, 2004.

[2] M. Sipos *et al.*, “Analyses of triaxial accelerometer calibration algorithms,” *IEEE Sens J*, vol. 12, no. 5, pp. 1157–1165, 2012, doi: 10.1109/JSEN.2011.2167319.

[3] M. Alam and J. Rohac, “Adaptive data filtering of inertial sensors with variable bandwidth,” *Sensors (Switzerland)*, vol. 15, no. 2, pp. 3282–3298, 2015, doi: 10.3390/s150203282.

[4] J. Farrell, *Aided navigation: GPS with high rate sensors*. McGraw-Hill, Inc., 2008.

[5] J. A. Farell, *Aided Navigation: GPS with High Rate Sensors*, vol. 1542. 2015. doi: 10.1017/CBO9781107415324.004.

[6] J. Rohac, J. M. Hansen, M. Alam, M. Sipos, T. A. Johansen, and T. I. Fossen, “Validation of nonlinear integrated navigation solutions,” *Annu Rev Control*, vol. 43, pp. 91–106, 2017, doi: 10.1016/j.arcontrol.2017.03.006.

[7] P.-J. Bristeau and N. Petit, “Navigation system for ground vehicles using temporally interconnected observers,” in *American Control Conference (ACC), 2011*, 2011, pp. 1260–1267.

[8] M. Alam, G. Moreno, M. Sipos, and J. Rohac, “INS / GNSS Localization Using 15 State Extended Kalman Filter,” in *International Conference in Aerospace for Young Scientists*, 2016, pp. 425–435. Accessed: Jan. 25, 2019. [Online]. Available: https://www.researchgate.net/publication/311616106

[9] D. Simon, “Kalman filtering with state constraints: a survey of linear and nonlinear algorithms,” *IET Control Theory & Applications*, vol. 4, no. 8, p. 1303, 2010, doi: 10.1049/iet-cta.2009.0032.

[10] H. Fourati and D. E. C. Belkhiat, “Multisensor attitude estimation: Fundamental concepts and applications,” *Multisensor Attitude Estimation: Fundamental Concepts and Applications*, pp. 1–580, Nov. 2016, doi: 10.1201/9781315368795.

[11] F. Gustafsson *et al.*, “Particle filters for positioning, navigation, and tracking,” *IEEE Transactions on Signal Processing*, vol. 50, no. 2, pp. 425–437, 2002, doi: 10.1109/78.978396.

[12] M. Alam, J. Whidborne, and M. Millidere, “Performance Analysis of eXogenous Kalman Filter for INS/GNSS Navigation Solutions,” *IFAC-PapersOnLine*, vol. 56, no. 2, pp. 11267–11272, Jan. 2023, doi: 10.1016/J.IFACOL.2023.10.319.

[13] National Transportation Safety Committee, “Aircraft Accident Investigation Report – Lion Mentari Airlines Boeing 737-8 (MAX) – Reg. PK-LQP - Report No: KNKT.1810.35.04,” West Java, Oct. 2018.

[14] Aircraft Accident Investigation Bureau, “Investigation Report on Accident To The B737-Max8 Reg. ET-AVJ Operated Ethiopian Airline - Report Number AI-01/19,” Dec. 2022.

[15] L. SANKARALINGAM and C. RAMPRASADH, “A comprehensive survey on the methods of angle of attack measurement and estimation in UAVs,” *Chinese Journal of Aeronautics*, vol. 33, no. 3. 2020. doi: 10.1016/j.cja.2019.11.003.

[16] P. Tian, H. Chao, H. P. Flanagan, S. G. Hagerott, and Y. Gu, “Design and evaluation of UAV flow angle estimation filters,” *IEEE Trans Aerosp Electron Syst*, vol. 55, no. 1, 2019, doi: 10.1109/TAES.2018.2852359.

[17] T. A. Johansen, A. Cristofaro, K. Sorensen, J. M. Hansen, and T. I. Fossen, “On estimation of wind velocity, angle-of-attack and sideslip angle of small UAVs using standard sensors,” in *2015*

International Conference on Unmanned Aircraft Systems, ICUAS 2015, 2015. doi: 10.1109/ICUAS.2015.7152330.

[18] RTCA, "Minimum Operational Performance Standards (MOPS) for Strapdown Attitude and Heading Reference Systems (AHRS) - RTCA DO-334," Washington, Mar. 2012.

[19] "Ekinox Series - Advanced Inertial Navigation Sensors - SBG Systems." Accessed: Dec. 03, 2023. [Online]. Available: https://www.sbg-systems.com/products/ekinox-series/#ekinox2-d_advanced_rtk_inertial_navigation_system

[20] "AHS-3000A/S Attitude Heading System | Collins Aerospace." Accessed: Dec. 03, 2023. [Online]. Available: https://www.collinsaerospace.com/what-we-do/industries/business-aviation/flight-deck/additional-flight-deck/attitude-and-heading/ahs3000as

Appendices

Appendix A

Innovation plots for the attitude estimator.

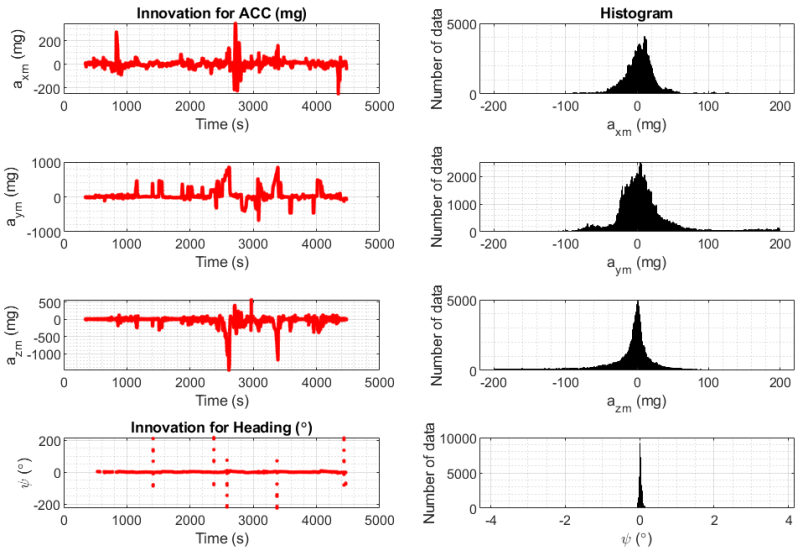

Fig. 8. Innovation plot for the attitude estimator.

The innovation plots in Fig. 8 have a normal distribution like shape around the zero-mean value.

Appendix B

Innovation plot for the Position/Velocity Air data estimator.

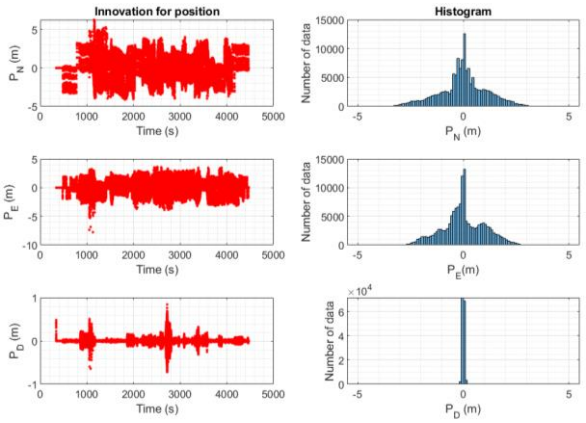

(a) Position innovation.

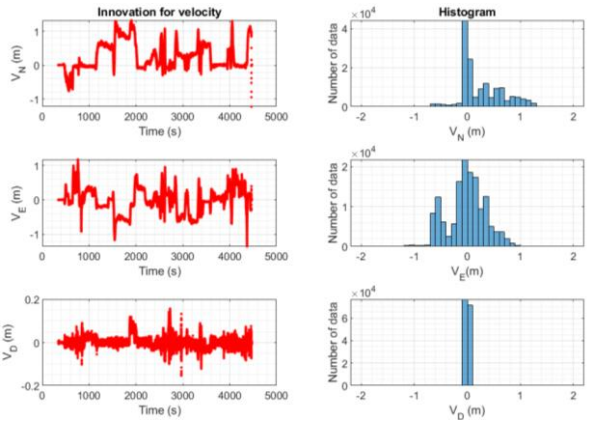

(b) Velocity innovation.

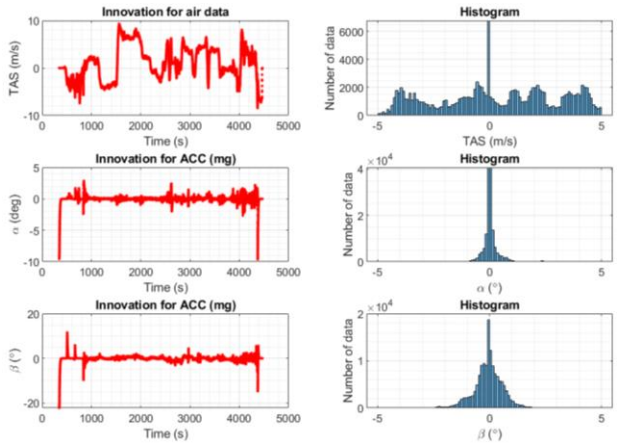

(c) Air data innovation.

Fig. 9. Innovation plots for the position/velocity air data estimator.

Fig. 9a has normal distribution like shape for position innovations around zero-mean value. In comparison in Fig. 9b the velocity estimates in V_N and V_E does not have normal distribution like shape due to value of measurement covariance being different.

Appendix C

This section provides the tuning parameters used in the estimation algorithm.

Attitude estimator

Measurement noise covariance

When compensation using accelerometer only:

$$R = \text{diag}[25mg, 25mg\ 25mg]$$

When compensation using accelerometer and heading from GNSS velocity:

$$R = \text{diag}[25mg, 25mg\ 25mg, 1.5^o]$$

Position/Velocity and Air data estimator

Measurement noise covariance

When compensating with GNSS position, velocity, and air data from pitot-static tube and AoA and AoS sensor:

$$R = \text{diag}[1m, 1m, 9m, 4m/s, 4m/s\ ,4m/s, 25m/s, 6.25^o, 6.25^o\ ]$$

Threshold value used in Section 2.2

These values are set from the observation of the aircraft dynamics.

Condition 1: 50 mg $< threshold_{ACC}$.

Condition 2: $5^o/s\ < threshold_{GYR}$.

Condition 3: $10^o/s < threshold_{ARS}$.